IEICE TRANSACTIONS

on Communications

DOI:10.23919/transcom.2024EBP3026

This advance publication article will be replaced by the finalized version after proofreading.

A PUBLICATION OF THE COMMUNICATIONS SOCIETY

The Institute of Electronics, Information and Communication Engineers

Kikai-Shinko-Kaikan Bldg., 5-8, Shibakoen 3chome, Minato-ku, TOKYO, 105-0011 JAPAN

PAPER

Reduction of fiber four-wave mixing generated from modulated lights by inserting dispersive elements

Ayano Inoue[†], ***nonmember***, **Koji Igarashi**[†], ***member***, **Shigehiro Takasaka**[††], ***member***, ***and*** **Kyo Inoue**[†], ***member***

SUMMARY Four-wave mixing (FWM) is a crucial impairment factor in optical wavelength-division-multiplexing (WDM) transmission systems over dispersion-shifted fibers. This paper presents an FWM suppression scheme that places dispersive elements (DEs) such as dispersion compensation fibers at optically repeating points in transmission lines. In a DE, the relative phase of the transmitted signal lights and the FWM light generated in the previous spans is shifted. Consequently, the FWM lights generated in each span are summed in random phases and the total FWM power at the end of the transmission lines is reduced from that in straight transmission lines with no DEs. We conduct proof-of-principle experiments to confirm the mechanism of the FWM reduction. Calculation for evaluating the FWM reduction ratio in a WDM transmission system is also presented.

key words: *Fiber four-wave mixing, suppression scheme, chromatic dispersion, modulated signal.*

1. Introduction

Four-wave mixing (FWM) is a nonlinear optical phenomenon that generates new wavelengths of light from two or three optical signals of different wavelengths [1]. This phenomenon can degrade wavelength-division-multiplexing (WDM) transmission systems, in which the generated FWM lights overlap onto the signal light and serve as noise [2, 3]. FWM is efficiently generated in dispersion-shifted fibers (DSFs) because the phase-matching condition, under which the nonlinear polarization wave and signal waves co-propagate in phase, is easily satisfied in DSFs [4]. Therefore, DSFs are not employed in optical transmission systems because FWM hinders WDM transmission. However, previously installed DSFs are still used in some transmission systems. The performance of such transmission systems would be improved if FWM generation could be reduced.

Conventionally, the use of non-zero dispersion fibers or the dispersion management has been known as a countermeasure against FWM in WDM systems over DSFs. However, non-zero dispersion fibers must be intentionally installed for this scheme. The use of the L band instead of the C band is also effective to mitigate FWM over DSF transmission lines [5]. However, this countermeasure wastes the C band or cannot be applied to the C-band transmission, for which the fiber attenuation is minimum and standard Erbium-doped fiber amplifiers are available.

On the above background, this paper presents a scheme to mitigate FWM in optical repeating transmission systems over DSFs, where WDM lights are positioned in the zero-dispersion wavelength of the DSFs in the worst case. Dispersive elements (DEs) such as dispersion compensation fibers (DCFs) are inserted into transmission lines. Through a DE, the relative phase between the nonlinear polarization wave and the FWM lights generated in the previous spans is shifted. Consequently, the phases of the FWM lights generated in each span are randomized, and the total FWM power is reduced from that in straight transmission lines without DEs. We analyze the FWM generation in transmission lines with DCFs and conduct proof-of-principle experiments. Subsequently, calculations for evaluating FWM reduction in WDM systems are presented.

2. Analysis

2.1 System model

The transmission system model considered in this study is illustrated in Fig. 1. It is an optically repeating system over DSFs, in which optical amplifiers are placed between the transmitter and receiver at equal intervals. The amplifier gain is set to a value that compensates for the transmission loss of one span. At the output of each amplifier, a DCF is placed as a DE, which introduces a phase shift between the nonlinear polarization wave and the FWM light, as will be described later. WDM signal lights with identical polarization states are assumed to be transmitted over this transmission line.

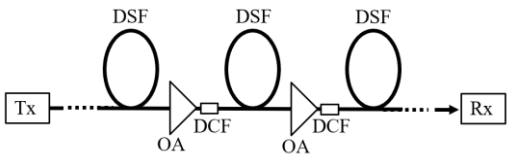

Fig. 1 Transmission system model. Tx: transmitter, Rx: receiver, DSF: dispersion-shifted fiber, OA: optical amplifier, DCF: dispersion compensation fiber.

†The authors are with Osaka University, Suita, 565-0871 Japan.
††The author is with Furukawa Electric Co. Ltd., Ichihara, 290-8555 Japan.

2.2 FWM generation

The FWM light at the receiver can be regarded as the sum of FWM lights generated in each span that linearly propagate to the receiver. We denote the amplitude of the FWM light generated in the kth span at position z by $A_F^{(k)}(z)$. This amplitude at the end of the kth span can be expressed as [6, 7]

$$A_F^{(k)}(z_k + L_0) = id\gamma A_1(z_k) A_2(z_k) A_3^*(z_k) \times \frac{1 - e^{-(\alpha - i\Delta\beta)L_0}}{\alpha - i\Delta\beta} e^{-(\alpha/2 - i\beta_F)L_0}, \quad (1)$$

where the FWM light generated at frequency $f_F = f_1 + f_2 - f_3$ is considered, where f_j is the signal-light frequency (j = 1 – 3); $A_j(z)$ denotes the signal light amplitude of frequency f_j at position z; γ is the nonlinear coefficient; d is the degeneracy factor, which is 2 for $f_1 \neq f_2$ and 1 for $f_1 = f_2$, $\Delta\beta \equiv \beta_1 + \beta_2 - \beta_3 - \beta_F$ denotes the phase mismatch in a DSF; β_j is the propagation constant for light of frequency f_j; α is the fiber loss coefficient; L_0 is the length of one span; and z_k denotes the position of the input of the kth span.

The signal light at position z_k can be expressed as

$$A_j(z_k) = A_{j0} \exp[i(k-1)(\beta_j L_0 + b_j L_d)], \quad (2)$$

where A_{j0} denotes the signal amplitude at z = 0, b_j is the propagation constant in a DCF for f_j frequency light, and L_d is the DCF length. Substituting Eq. (2) into Eq. (1) yields

$$A_F^{(k)}(z_k + L_0) = id\gamma A_{10} A_{20} A_{30}^* \frac{1 - e^{-(\alpha - i\Delta\beta)L_0}}{\alpha - i\Delta\beta} e^{-(\alpha/2 - i\beta_F)L_0} \times \exp[i(k-1)\{(\beta_F + \Delta\beta)L_0 + (b_F + \Delta b)L_d\}], \quad (3)$$

where $\Delta b \equiv b_1 + b_2 - b_3 - b_F$ denotes the phase mismatch in a DCF.

The FWM light generated in the kth span propagates linearly to the receiver. Its amplitude at the receiver can be expressed as

$$A_F^{(k)}(\text{end}) = A_F^{(k)}(z_k + L_0) \exp[i(N-k)(\beta_F L_0 + b_F L_d)], \quad (4)$$

where N is the total number of spans from the transmitter to the receiver. Substituting Eq. (3) into Eq. (4) and expanding the formula, we obtain the following expression for the FWM light generated in the kth span and reaching the receiver:

$$A_F^{(k)}(\text{end}) = id\gamma A_{10} A_{20} A_{30}^* \frac{1 - e^{(-\alpha + i\Delta\beta)L_0}}{\alpha - i\Delta\beta} e^{(-\alpha/2 + iN\beta_F)L_0} \times e^{i(N-1)\beta_F L_d} e^{i(k-1)(\Delta\beta L_0 + \Delta b L_d)}. \quad (5)$$

The total FWM light amplitude at the receiver, A_F, is expressed by the sum of FWM lights generated in each span and reaching the receiver, as shown below:

$$A_F = \sum_{k=1}^{N} A_F^{(k)}(\text{end}) = id\gamma A_{10} A_{20} A_{30}^* \frac{1 - e^{(-\alpha + i\Delta\beta)L_0}}{\alpha - i\Delta\beta} e^{(-\alpha/2 + iN\beta_F)L_0} e^{i(N-1)\beta_F L_d} \times \sum_{k=1}^{N} e^{i(k-1)(\Delta\beta L_0 + \Delta b L_d)}. \quad (6)$$

Subsequently, the FWM power at the receiver, P_F, is expressed as

$$P_F = |A_F|^2 = (d\gamma)^2 P_0^3 e^{-\alpha L_0} \left| \frac{1 - e^{(-\alpha + i\Delta\beta)L_0}}{\alpha - i\Delta\beta} \right|^2 \cdot \left| \sum_{k=1}^{N} e^{i(k-1)(\Delta\beta L_0 + \Delta b L_d)} \right|^2 = (d\gamma)^2 P_0^3 e^{-\alpha L_0} \eta(\Delta\beta) \frac{\sin^2[N(\Delta\beta L_0 + \Delta b L_d)/2]}{\sin^2[(\Delta\beta L_0 + \Delta b L_d)/2]}, \quad (7)$$

with

$$\eta(\Delta\beta) \equiv \frac{(1 - e^{-\alpha L_0})^2 + 4e^{-\alpha L_0} \sin^2(\Delta\beta L_0/2)}{\alpha^2 + \Delta\beta^2},$$

where $P_0 = |A_{j0}|^2$. For L_d = 0, i.e., the case without DCFs, this equation can be rewritten as [8]

$$P_F(L_d = 0) = (d\gamma)^2 P_0^3 e^{-\alpha L_0} \eta(\Delta\beta) \frac{\sin^2[N\Delta\beta L_0/2]}{\sin^2[\Delta\beta L_0/2]}. \quad (8)$$

2.3 FWM reduction

Using Eqs. (7) and (8), the power ratio of the FWM light with and without DCFs, R, can be evaluated as

$$R = \frac{P_F(L_d \neq 0)}{P_F(L_d = 0)} = \frac{\sin^2[N(\Delta\beta L_0 + \Delta b L_d)/2]}{\sin^2[(\Delta\beta L_0 + \Delta b L_d)/2]} \cdot \frac{\sin^2[\Delta\beta L_0/2]}{\sin^2[N\Delta\beta L_0/2]}. \quad (9)$$

For $\Delta\beta L_0$ = 0, i.e., the case where the phase matching condition is satisfied in the DSFs, Eq. (9) can be rewritten as

$$R(\Delta\beta = 0) = \frac{1}{N^2} \cdot \frac{\sin^2(N\Delta b L_d/2)}{\sin^2(\Delta b L_d/2)}. \quad (10)$$

This expression indicates that R takes a value from 0 to 1, depending on $\Delta b L_d$. Therefore, the ratio R can be used as an index to represent the FWM power reduction by inserting DCFs.

The reduction ratio, R, depends on $\Delta b L_d$, as shown in Eq. (9), which can be expressed as [9]

$$\Delta b L_d = \frac{2\lambda^2 \pi}{c} D_d L_d (f_1 - f_3)(f_2 - f_3), \quad (11)$$

where λ is the light wavelength, c is the light velocity, and D_d is the dispersion parameter of a DCF. Equations (10) and (11) indicate that the reduction ratio varies periodically as a function of the signal frequencies, such as R = 1 at the signal frequencies satisfying $\Delta b L_d/2 = m\pi$, where m is an integer.

Here, we consider the frequency interval between the neighboring peaks of R for FWM generation at $f_F = 2f_1 - f_3$ from signal lights of frequencies f_1 and f_3. For this partially

degenerate FWM process, Eq. (11) can be rewritten as

$$\Delta bL_{\mathrm{d}} = \frac{2\lambda^2\pi}{c} D_{\mathrm{d}} L_{\mathrm{d}} \Delta f^2 , \qquad (12)$$

where $\Delta f = f_1 - f_3$ is the frequency separation between the two signal lights. Denoting the frequency interval as f_π, the following equation is obtained:

$$\frac{2\lambda^2\pi}{c} D_{\mathrm{d}} L_{\mathrm{d}} (\Delta f + f_\pi)^2 - \frac{2\lambda^2\pi}{c} D_{\mathrm{d}} L_{\mathrm{d}} \Delta f^2 = 2\pi , \quad (13)$$

from which f_π is expressed as

$$f_\pi \approx \frac{c}{2\lambda^2 D_{\mathrm{d}} L_{\mathrm{d}} \Delta f} , \qquad (14)$$

where $f_\pi << \Delta f$ is assumed. For example, when $D_{\mathrm{d}} = -160$ ps/km-nm, $L_{\mathrm{d}} = 2$ km, and $\Delta f = 100$ GHz, f_π is approximately 2 GHz.

In general, the frequency spectrum of a modulated signal light is broadened around the carrier frequency according to signal modulation. Subsequently, the frequency separation Δf is broadened around the mean value of the modulated signal lights. When this frequency broadening is larger than the frequency interval f_π, the FWM reduction ratio R is averaged over the frequency separation as

$$\langle R \rangle = \left\langle \frac{\sin^2[N(\Delta\beta L_0 + \Delta bL_{\mathrm{d}})/2]}{\sin^2[(\Delta\beta L_0 + \Delta bL_{\mathrm{d}})/2]} \right\rangle \frac{\sin^2[\Delta\beta L_0/2]}{\sin^2[N\Delta\beta L_0/2]} , \qquad (15)$$

where $\langle\ \rangle$ represents the average over the frequency separation Δf or ΔbL_{d}. The average term in Eq. (15) is calculated as [Appendix]

$$\left\langle \frac{\sin^2[N(\Delta\beta L_0 + \Delta bL_{\mathrm{d}})/2]}{\sin^2[(\Delta\beta L_0 + \Delta bL_{\mathrm{d}})/2]} \right\rangle = N . \qquad (16)$$

Subsequently, Eq. (15) is rewritten as

$$\langle R \rangle = N \frac{\sin^2[\Delta\beta L_0/2]}{\sin^2[N\Delta\beta L_0/2]} . \qquad (17)$$

For $\Delta\beta L_0 \approx 0$, this equation becomes

$$\langle R(\Delta\beta L_0 \approx 0) \rangle = \frac{1}{N} . \qquad (18)$$

The analysis above indicates that the FWM generation is reduced by a factor of the number of repeating spans in systems where the phase matching condition is satisfied in the DSFs.

3. Experiment

To confirm the mechanism of the FWM reduction described in the previous section, we conducted a proof-of-principle experiment using the setup shown in Fig. 2. Two wavelength lights were combined via an optical coupler, optically amplified, and incident into two cascaded 2.5-km DSFs with an identical zero-dispersion wavelength, between which an optical amplifier and a DCF with a dispersion parameter of -164 ps/km-nm and a length of 2.0 or 0.5 km, were inserted.

The DSFs with a length of 2.5 km were employed simply because they were available in our laboratory. The basic ideal of the proposed scheme reducing the FWM power at the end of the transmission line is to randomize the phase relationship between FWM lights generated in each repeating span. Therefore, the FWM power generated in each span, or the span length, is irrelevant to the reduction ratio, and any length of DSFs could be used in the proof-of-principle experiment.

In the above setup, one light was a continuous wave (CW), called "pump light" hereafter, whose wavelength was fixed at the zero-dispersion wavelength of the DSFs. The other light was generated from a wavelength-tunable LD, called "signal light" hereafter, which was CW, quadrature-phase-shift-keying (QPSK) modulated at 12.5 Gbaud, or on-off-keying (OOK) modulated at 12.5 Gbps. The signal wavelength was varied in the longer wavelength side of the pump light. The optical paths from the two light sources to the coupler were constructed using polarization-maintaining fibers, owing to which the two lights were incident to the DSFs in an identical polarization state. The amplifier gain between the DSFs was adjusted such that the optical powers at the inputs of the first and second DSFs were identical as approximately 11 dBm.

The output from the DSFs was incident to an optical spectrum analyzer, and the FWM light power generated in the shorter wavelength side of the pump light was measured. This is because the proposed reduction scheme is effective for FWM satisfying the phase matching condition $\Delta\beta = 0$, as indicated by Eqs. (9) and (10), and the FWM light at the shorter wavelength side satisfied the phase matching condition in the above wavelength allocation.

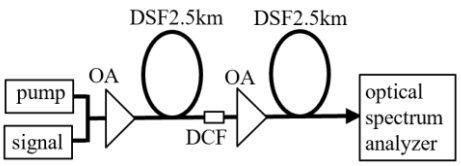

Fig. 2 Experimental setup. DSF: dispersion-shifted fiber, OA: optical amplifier, and DCF: dispersion-compensation fiber.

For the above system condition, the FWM reduction ratio for CW lights can be expressed from Eq. (10) as

$$R(N = 2, \Delta\beta L_0 = 0) = \cos^2(\Delta bL_{\mathrm{d}}/2) , \qquad (19)$$

where

$$\Delta b = \frac{2\lambda^2\pi}{c} D_{\mathrm{d}} (f_{\mathrm{s}} - f_{\mathrm{p}})^2 . \qquad (20)$$

In the present experiment, the FWM lights generated in the first and second DSFs interfered with each other at the output end. Therefore, a dual-beam interference pattern would be observed as indicated in Eq. (19). We conducted the following measurement to confirm the formula.

First, a 2.0-km DCF was inserted, and the CW signal was incident. The observed output spectrum is shown in Fig. 3, where the outputs with and without the DCF are indicated by solid and dashed lines, respectively. In this measurement, the signal light wavelength was carefully chosen at which the FWM power was most effectively reduced. The FWM light in the shorter wavelength side of the pump light was our concern, whose power

was significantly reduced by the DCF. On the other hand, the power reduction of the FWM generated in the longer wavelength side was not so significant, because the phase matching condition was not satisfied, i.e., $\Delta\beta \neq 0$, for this FWM light.

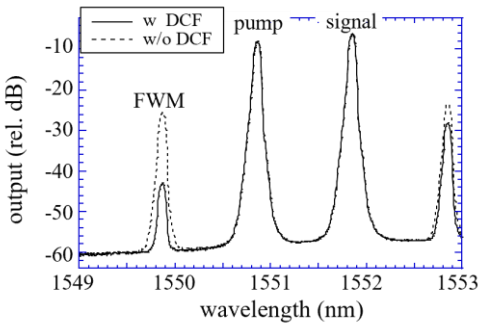

Fig. 3 Output spectrum. DCF length was 2.0 km and signal light was CW. Solid and dashed lines denote outputs with and without DCF, respectively.

The measurement above was performed while the signal-light wavelength was changed, from which the relative FWM power as a function of the frequency separation between the signal and pump lights was plotted. The optical frequency was quoted from the value displayed in the wavelength-tunable LD. The results are shown in Fig. 4(a); additionally, the FWM reduction ratio R calculated using Eq. (19) is shown in Fig. 4(b). As expected from the analytical formula, a periodic output was observed in the experiment, although the extinction ratio was insufficient especially for large frequency separations, and the absolute value of the frequency separation was different between the experimental and calculation results by approximately 1 GHz.

The insufficient extinction ratio was owing to the experimental condition of measuring points in one period being few. In the measurement, we focused on to observe a periodicity or an interference pattern, without caring for the extinction ratio, and thus did not finely change the signal light frequency, being afraid that the experimental conditions varied during the measurement. Subsequently, the number of measuring points were not sufficient to observe a high extinction ratio. The absolute frequency difference between the experiment and calculation might be because the frequency-monitoring system equipped in the wavelength-tunable LD did not have an accuracy within 1 GHz, and the actual frequency differed from the value displayed on the LD module.

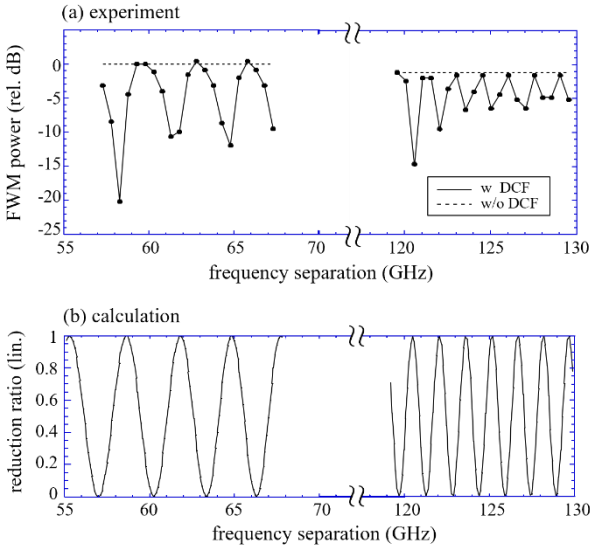

Fig. 4 FWM power as a function of frequency separation between signal and pump lights. DCF length was 2.0 km and signal light was CW.

Next, the signal light was QPSK modulated instead of CW. The output spectrum and the measured FWM power are shown in Figs. 5 and 6, respectively. Figure 5 indicates that the signal-light spectrum was broadened owing to the QPSK modulation, as was the FWM light. Owing to this spectrum broadening, the FWM power was averaged over the frequency separation and observed to be almost constant at a value that was 3 – 4 dB less than the FWM power without the DCF, as shown in Fig. 6. This experimental result confirmed the FWM reduction for the modulated signals, as suggested by Eq. (18).

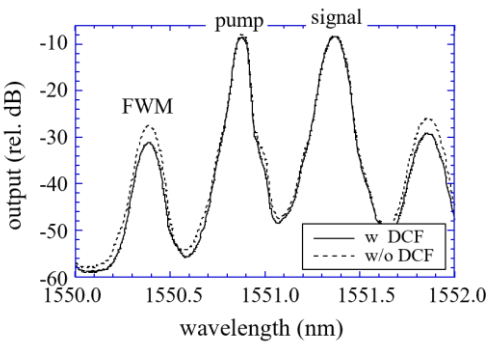

Fig. 5 Output spectrum. DCF length was 2.0 km and signal light was QPSK modulated. Solid and dashed lines denote outputs with and without DCF, respectively.

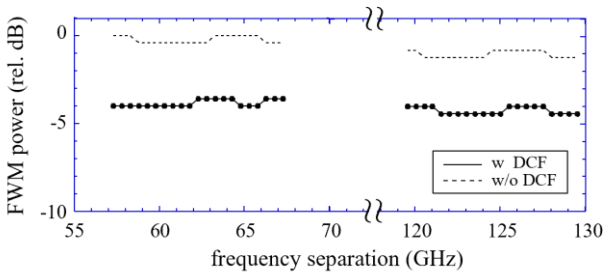

Fig. 6 FWM power as a function of frequency separation between signal and pump lights. DCF length was 2.0 km and signal light was QPSK modulated at 12.5 Gbaud.

Next, the signal light was OOK modulated instead of QPSK modulated. The measured FWM power as a function of frequency separation is shown in Fig. 7. In contrast to the result for the QPSK modulated signal shown in Fig. 6, a periodic FWM output was observed even though the modulated light was incident. However, the depth of the periodicity was smaller than that for the CW signal shown in Fig. 4, which is an intermediate property between those of the CW and QPSK signals. This might be because the spectrum of the OOK-modulated light contained a peak at the carrier frequency and was not uniformly broadened, unlike the QPSK signal. Therefore, the OOK signal was in an intermediate state between the CW and QPSK signals in terms of the spectrum, for which the FWM power was partially averaged. As shown in Fig. 7, the discrepancy between the peak FWM level with and without the DCF was larger in the frequency region of 120 – 130 GHz than in the range of 60 – 70 GHz. This might be because the frequency period in the former frequency region was narrower and the averaging effect was more effective.

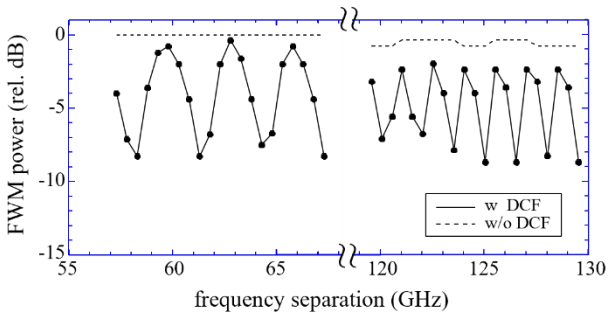

Fig. 7 FWM power as a function of frequency separation between signal and pump lights. DCF length was 2.0 km and signal light was OOK modulated at 12.5 Gbps.

Subsequent to the use of a 2.0-km DCF, we examined a DCF with a length of 0.5 km. The results for the CW signal are shown in Fig. 8, where the measured FWM power and FWM reduction ratio calculated using Eq. (19) are plotted in (a) and (b), respectively. Frequency periodicity was observed, similar to the results for the 2.0-km DCF shown in Fig. 4; however, the period was four times larger than that for the 2.0-km DCF, thus corresponding to the fact that the 0.5-km DCF is four times shorter than the 2.0-km DCF.

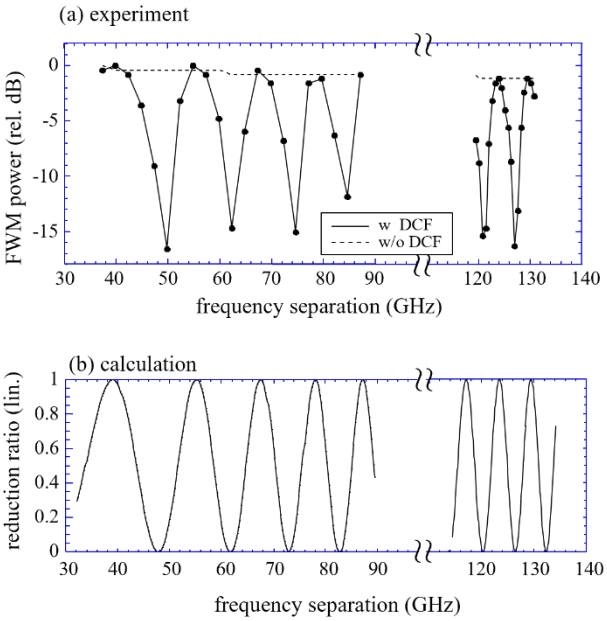

Fig. 8 FWM power as a function of frequency separation between signal and pump lights. DCF length was 0.5 km and signal light was CW.

Additionally, we examined the 12.5-Gbaud QPSK signal for the system with a 0.5-km DCF; the result is shown in Fig. 9. In contrast to the result of the system with a 2.0-km DCF, periodicity was observed in the frequency region of 40 – 90 GHz, even when the signal light was QPSK modulated. This is attributed to the insufficient averaging effect arising from the wide frequency period shown in Fig. 8. The experimental results above based on the 0.5-km DCF indicate that the DCF length should be selected appropriately by considering on the frequency separation and signal modulation bandwidth to obtain the averaging effect.

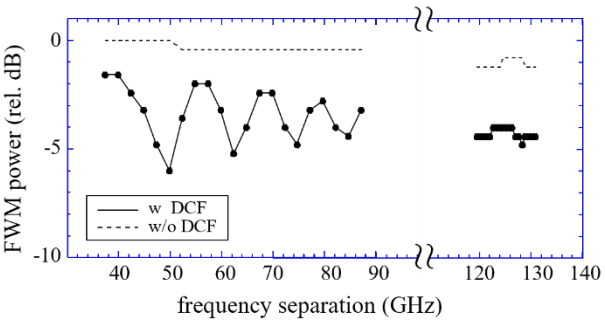

Fig. 9 FWM power as a function of frequency separation between signal and pump lights. DCF length was 0.5 km and signal light was QPSK modulated at 12.5 Gbps.

The experimental results above showed the FWM generation characteristics expected from the theoretical analysis in the previous section, confirming the mechanism of FWM reduction by inserting DEs.

4. FWM reduction in WDM system

The analytical formula indicating the FWM suppression is presented in Section 2, and its validity is experimentally confirmed in Section 3. Subsequently, this section calculates the FWM reduction ratio in an optically repeating WDM transmission system over DSFs, using the formula derived in Section 2 and experimentally confirmed in Section3.

Based on Eq. (7), the total FWM power generated at the sth channel in a WDM transmission system with DEs can be expressed as

$$P_{\mathrm{F}} = 4\kappa \sum_{p,q,r} \eta(\Delta\beta_{pqr}) \frac{\sin^2[N(\Delta\beta_{pqr}L_0 + \Delta b_{pqr}L_{\mathrm{d}})/2]}{\sin^2[(\Delta\beta_{pqr}L_0 + \Delta b_{pqr}L_{\mathrm{d}})/2]} + \kappa \sum_{p,r} \eta(\Delta\beta_{ppr}) \frac{\sin^2[N(\Delta\beta_{ppr}L_0 + \Delta b_{ppr}L_{\mathrm{d}})/2]}{\sin^2[(\Delta\beta_{ppr}L_0 + \Delta b_{ppr}L_{\mathrm{d}})/2]}, \quad (21)$$

where $\{p, q, r\}$ indicate the channel numbers; $\kappa \equiv \gamma^2 P_0^3 \exp(-\alpha L_0)$; and the fiber dispersion is assumed to be uniform along the transmission lines, considering the worst-case scenario. The first summation represents the FWM power generated from nondegenerate processes satisfying $f_s = f_p + f_q - f_r$, and the second summation represents that from partially degenerate processes satisfying $f_s = 2f_p - f_r$.

Provided that DCFs of an appropriate length, with which the spectrum bandwidth of the FWM light is sufficiently wider than the frequency period, e.g., 2.0-km DCFs for 12.5 Gbaud QPSK systems, are used, Eq. (21) is averaged as follows:

$$\begin{aligned} <P_{\mathrm{F}}> &= 4\kappa \sum_{p,q,r} \eta(\Delta\beta_{pqr}) \left\langle \frac{\sin^2[N(\Delta\beta_{pqr}L_0 + \Delta b_{pqr}L_{\mathrm{d}})/2]}{\sin^2[(\Delta\beta_{pqr}L_0 + \Delta b_{pqr}L_{\mathrm{d}})/2]} \right\rangle \\ &\quad + \kappa \sum_{p,r} \eta(\Delta\beta_{ppr}) \left\langle \frac{\sin^2[N(\Delta\beta_{ppr}L_0 + \Delta b_{ppr}L_{\mathrm{d}})/2]}{\sin^2[(\Delta\beta_{ppr}L_0 + \Delta b_{ppr}L_{\mathrm{d}})/2]} \right\rangle \\ &= \kappa N \left\{ 4 \sum_{p,q,r} \eta(\Delta\beta_{pqr}) + \sum_{p,r} \eta(\Delta\beta_{ppr}) \right\}. \end{aligned} \quad (22)$$

Subsequently, the FWM reduction ratio for QPSK-modulated signal lights, $<R> = <P_{\mathrm{F}}(L_{\mathrm{d}} \neq 0)> / P_{\mathrm{F}}(L_{\mathrm{d}} = 0)$, is evaluated as

$$<R> = N \left\{ 4 \sum_{p,q,r} \eta(\Delta\beta_{pqr}) + \sum_{p,r} \eta(\Delta\beta_{ppr}) \right\} \times \left\{ 4 \sum_{p,q,r} \eta(\Delta\beta_{pqr}) \frac{\sin^2[N\Delta\beta_{pqr}L_0/2]}{\sin^2[\Delta\beta_{pqr}L_0/2]} + \sum_{p,r} \eta(\Delta\beta_{ppr}) \frac{\sin^2[N\Delta\beta_{ppr}L_0/2]}{\sin^2[\Delta\beta_{ppr}L_0/2]} \right\}^{-1}. \quad (23)$$

The phase mismatch in this equation is expressed as [3]

$$\Delta\beta_{pqr} = \frac{\pi\lambda^4 D_{\mathrm{cc}}}{c^2}(f_p + f_q - 2f_0)(p - r)(q - r)\Delta f^2, \quad (24a)$$

$$\Delta\beta_{ppr} = \frac{2\pi\lambda^4 D_{\mathrm{cc}}}{c^2}(f_p - f_0)(p - r)^2 \Delta f^2, \quad (24b)$$

where $D_{\mathrm{cc}} = \mathrm{d}D_{\mathrm{c}}/\mathrm{d}\lambda$ with D_{c} being the dispersion parameter of the DSFs; Δf is the channel frequency spacing; and f_0 is the zero-dispersion frequency of the DSFs.

Using Eq. (23), we calculated the FWM reduction ratio as a function of the number of spans for the center channel in a 100-GHz spaced 11-channel WDM system. The span length was 80 km, and the center channel was assumed to be positioned at the zero-dispersion wavelength of the transmission fibers, considering the worst-case scenario. The signal lights were assumed to have a single and identical polarization state. However, the result obtained under this condition of the polarization state would be applicable to polarization-multiplexed systems, because the FWM reduction mechanism of randomizing the relative phases of FWM lights generated in each span works independently on the two orthogonal polarization components and the FWM reduction is obtained in each polarization state.

The results are presented in Fig. 10. As shown, the FWM reduced efficiently as the number of spans increased. Although the previous section indicated that the reduction ratio was $1/N$ for a phase-matched FWM component in an N-span system, the reduction ratio shown in Fig. 10 did not reach this level. This is because FWM in WDM systems includes components that do not satisfy the phase-matching condition, i.e., $\Delta\beta_{pqr} \neq 0$, and the efficiency of FWM reduction for those components is not comparable to that for phase-matched components.

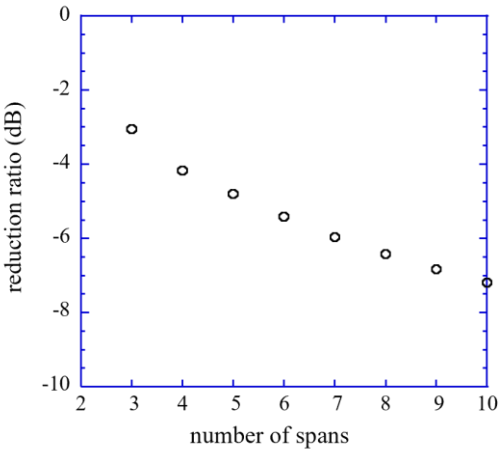

Fig. 10 FWM reduction ratio at center channel, positioned at zero-dispersion wavelength of transmission fibers, in 11-channel WDM system. Channel spacing was 100 GHz and repeater spans was 80 km.

In the last of this section, we briefly discuss how the FWM power reduction improves the WDM transmission performance. In general, FWM lights overlapped onto signal light serve as noise lights. Therefore, the reduction of the FWM power by x dB is equivalent to the improvement of the optical signal-to-noise ratio (OSNR) by x dB, roughly speaking. Subsequently, the OSNR penalty owing to FWM is expected to be improved by x dB in the BER performance.

5. Conclusion

A scheme for FWM reduction in optically repeating WDM transmission systems over DSFs was presented. DEs such as DCFs were inserted at repeating points, through which the relative phase between the transmitted signal lights and FWM lights generated in the previous spans was shifted. Consequently, FWM lights generated in each span overlapped in random phases, and the total FWM power at the receiver was lower than that in systems with no DEs. Proof-of-principle experiments were conducted, and the results confirmed the FWM reduction mechanism above. Calculation for evaluating the reduction ratio in WDM systems was presented.

Appendix

In this section, we derive Eq. (16). First, we introduce variable $x = (\Delta\beta L_0 + \Delta b L_d)/2$ to simplify the left-hand side of Eq. (16) as follows:

$$S_N = \left\langle \frac{\sin^2[N(\Delta\beta L_0 + \Delta b L_d)/2]}{\sin^2[(\Delta\beta L_0 + \Delta b L_d)/2]} \right\rangle = \left\langle \left\{ \frac{\sin(Nx)}{\sin x} \right\}^2 \right\rangle. \tag{26}$$

For $N = 2$ and 3, S_N can be calculated as

$$S_2 = \left\langle \left\{ \frac{\sin(2x)}{\sin x} \right\}^2 \right\rangle = 4\left\langle \cos^2 x \right\rangle = 2 \tag{27}$$

and

$$S_3 = \left\langle \left\{ \frac{\sin(3x)}{\sin x} \right\}^2 \right\rangle = \left\langle \{1 + 2\cos(2x)\}^2 \right\rangle = 3. \tag{28}$$

Next, we calculate S_N for larger values of N, through which the following expressions are supposed to be satisfied:

$$\frac{\sin(Nx)}{\sin x} = 2\sum_{k=1}^{N/2} \cos[(2k-1)x] \tag{29a}$$

for even N, and

$$\frac{\sin(Nx)}{\sin x} = 1 + 2\sum_{k=1}^{(N-1)/2} \cos(2kx) \tag{29b}$$

for odd N.

Subsequently, we prove Eq. (29) using mathematical induction. First, Eq. (29) is assumed to be satisfied for $N - 1$. Subsequently, $\sin(Nx)/\sin(x)$ is developed as follows:

$$\begin{aligned}
\frac{\sin(Nx)}{\sin x} &= \frac{1}{\sin x}\{\sin[(N-1)x]\cos x + \cos[(N-1)x]\sin x\} \\
&= \left\{1 + 2\sum_{k=1}^{(N-2)/2} \cos(2kx)\right\}\cos x + \cos[(N-1)x] \\
&= \cos x + \sum_{k=1}^{N/2-1} \{\cos[2(k+1)x] + \cos[2(k-1)x]\}x \\
&\quad + \cos[(N-1)x] \\
&= 2\sum_{k=1}^{N/2} \cos[(2k-1)x]
\end{aligned} \tag{30a}$$

for even N, and

$$\begin{aligned}
\frac{\sin(Nx)}{\sin x} &= \frac{1}{\sin x}\{\sin[(N-1)x]\cos x + \cos[(N-1)x]\sin x\} \\
&= 2\sum_{k=1}^{(N-1)/2} \cos[(2k-1)x]\cos x + \cos[(N-1)x] \\
&= \sum_{k=1}^{(N-1)/2} \{\cos(2kx) + \cos[2(k-1)x]\} \\
&\quad + \cos[(N-1)x] \\
&= \sum_{k=1}^{(N-1)/2} \cos(2kx) + 1 + \sum_{k=2}^{(N-1)/2} \cos[2(k-1)x] \\
&\quad + \cos\left[2 \cdot \frac{N-1}{2} \cdot x\right] \\
&= 1 + 2\sum_{k=1}^{(N-1)/2} \cos(2kx)
\end{aligned} \tag{30b}$$

for odd N, where Eq. (29) with $N - 1$ is applied. Eq. (30) indicates that Eq. (29) is satisfied provided that it is satisfied for $N - 1$. Futhermore, the validity of Eq. (29) for $N = 1$ and 2 are confirmed in Eqs. (27) and (28), respectively. Therefore, Eq. (29) is satisfied for any N.

Using Eq. (29), we can derive Eq. (26) as

$$\begin{aligned}
S_N &= 4\left\langle \left\{ \sum_{k=1}^{N/2} \cos[(2k-1)x] \right\}^2 \right\rangle \\
&= 4\left\langle \sum_{k=1}^{N/2} \cos^2[(2k-1)x] \right\rangle \\
&\quad + 8\left\langle \sum_{k<k'} \cos[(2k-1)x]\cos[(2k'-1)x] \right\rangle \\
&= N
\end{aligned} \tag{31a}$$

for even N, and

$$\begin{aligned}
S_N &= \left\langle \left\{ 1 + 2\sum_{k=1}^{(N-1)/2} \cos(2kx) \right\}^2 \right\rangle \\
&= \left\langle 1 + 4\sum_{k=1}^{(N-1)/2} \cos^2(2kx) \right\rangle \\
&\quad + 4\left\langle \sum_{k<k'} \cos(2kx)\cos(2k'x) \right\rangle \\
&= N
\end{aligned} \tag{31b}$$

for odd N. Therefore, Eq. (16) is derived.

References

[1] G. P. Agrawal, Nonlinear Fiber Optics, Academic Press, San Diego, 2001.
[2] R. W. Tkach, A. R. Chraplyvy, F. Forghieri, A. H. Gnauck, and R. M. Derosier, "Four-photon mixing and high-speed WDM systems," J. Lightw. Technol. vol. 13, no. 5, pp. 841–849, May 1995.
[3] K. Inoue, K. Nakanishi, K. Oda, and H. Toba, "Crosstalk and power penalty due to fiber four-wave mixing in multichannel transmissions," J. Lightw. Technol. vol. 12, no. 8, pp. 1423-1439, Aug. 1994.
[4] K. Inoue, "Four-wave mixing in an optical fiber in the zero-dispersion region," J. Lightw. Technol., vol. 10, no. 11, pp. 1553–1561, Nov. 1992.
[5] M. Jinno, T. Sakamoto, J. Kani, S. Aisawa, K. Oda, M. Fukui, H. Ono, and K. Oguchi, "First demonstration of 1580 nm wavelength band WDM transmission for doubling usable bandwidth and suppressing FWM in DSF," Electron. Lett., vol. 33, no. 10, pp. 882-883, May 1997.
[6] K. O. Hill, D. C. Johnson, B. S. Kawasaki, and R. I. MacDonald, "cw three-wave mixing in single-mode optical fibers," J. Appl. Phys. vol. 49, no. 10, pp. 5098–5106, Oct. 1978.
[7] K. Inoue, "Fiber four-wave mixing in multi-amplifier systems with nonuniform chromatics dispersion," J. Lightw. Technol., vol. 13, no. 1, pp. 88–93, Jan. 1995.
[8] K. Inoue, "Phase-mismatching characteristic of four-wave mixing in fiber lines with multistage optical amplifiers," Opt. Lett., vol. 17, no. 11, pp. 801–803, June 1992.
[9] N. Shibata, R. P. Braun, and R. G. Waarts, "Phase-mismatch dependence of efficiency of wave generation through four-wave mixing in a single-mode optical fiber," IEEE J. Quantum Electron. vol. QE-23, no. 7, pp. 1205–1210, July 1987.

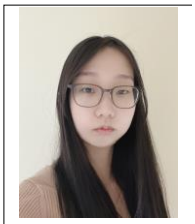

Ayano Inoue is an undergraduate student of the School of Engineering, Osaka University.

Koji Igarashi received the B.E. degree in electrical and computer engineering from Yokohama National University, Yokohama, Japan, in 1997, and the M.E. and Ph.D. degrees in electronic engineering from the University of Tokyo, Tokyo, Japan, in 1999 and 2002, respectively. He was with the Furukawa Electric Corporation, Ltd. from 2002 to 2004, the University of Tokyo from 2004 to 2011, and KDDI R&D Laboratories, Inc. from 2012 to 2013. He is currently an Associate Professor at Osaka University, Osaka, Japan. His current works include high-capacity long-haul optical fiber transmission systems, signal processing for coherent optical communication systems, and optical fibers devices for space-division multiplexed optical transmission systems.

Shigehiro Takasaka received B.S., M.S. and the Ph.D. degrees in Physics from Hokkaido University, Sapporo, Japan, in 1994, 1996, and 1999, respectively. He was a postdoctoral fellow of The University of Tokyo from 1999 to 2002. He joined Furukawa Electric Co., Ltd., Tokyo, Japan in 2002. He has been engaged in research and development of optical fiber applications such as nonlinear optical signal processing and fiber amplifiers. He was also a manager of Sakigake project on PRESTO, JST, Kawaguchi, Japan from 2004 to 2008. He is a senior researcher of optical application section of Photonics Laboratories., and a senior member of IEEE photonics society.

Kyo Inoue received the B.S. and M.S. degrees in applied physics in 1982 and 1984, respectively, and the Ph.D. degree in electrical engineering from Tokyo University, Tokyo, Japan, in 1997.
From 1984 to 2005, he was with Nippon Telegram and Telephone Corporation, where his work involved optical communications and quantum communications.
He is currently a Professor at Osaka University, Osaka, Japan.